Reproducibility of Measurements of Regional Myocardial Blood Flow in a Model of Coronary Artery Disease: Comparison of $H_2{}^{15}O$ and $^{13}NH_3$ PET Techniques

Panithaya Chareonthaitawee[1], Stuart D. Christenson[1], Jill L. Anderson[2], Brad J. Kemp[3], David O. Hodge[4], Erik L. Ritman[2], and Raymond J. Gibbons[1]

[1]Division of Cardiovascular Diseases, Mayo Clinic and Mayo Clinic College of Medicine, Rochester, Minnesota; [2]Department of Physiology and Biomedical Engineering, Mayo Clinic and Mayo Clinic College of Medicine, Rochester, Minnesota; [3]Division of Nuclear Medicine, Mayo Clinic and Mayo Clinic College of Medicine, Rochester, Minnesota; and [4]Division of Biostatistics, Mayo Clinic and Mayo Clinic College of Medicine, Rochester, Minnesota

PET absolute myocardial blood flow (MBF) with $H_2{}^{15}O$ and $^{13}NH_3$ are widely used in clinical and research settings. However, their reproducibility with a 16-myocardial segment model has not been examined in chronic coronary artery disease (CAD). We examined the short-term reproducibility of PET $H_2{}^{15}O$ MBF and PET $^{13}NH_3$ MBF in an animal model of chronic CAD. **Methods:** Twelve swine (mean weight ± SD, 38 ± 5 kg) underwent percutaneous placement of a copper stent in the mid circumflex coronary artery, resulting in an intense inflammatory fibrotic reaction with luminal stenosis at 4 wk. Each animal underwent repeated resting MBF measurements by PET $H_2{}^{15}O$ and PET $^{13}NH_3$. Attenuation-corrected images were analyzed using commercial software to yield absolute MBF (mL/min/g) in 16 myocardial segments. MBF was also normalized to the rate·pressure product (RPP). **Results:** By Bland–Altman reproducibility plots, the mean difference was 0.01 ± 0.18 mL/min/g and 0.01 ± 0.11 mL/min/g, with confidence limits of ±0.36 and ±0.22 mL/min/g for uncorrected regional PET $H_2{}^{15}O$ MBF and for uncorrected regional PET $^{13}NH_3$ MBF, respectively. The repeatability coefficient ranged from 0.09 to 0.43 mL/min/g for $H_2{}^{15}O$ and from 0.09 to 0.18 mL/min/g for $^{13}NH_3$ regional MBF. RPP correction did not improve reproducibility for either PET $H_2{}^{15}O$ or PET $^{13}NH_3$ MBF. The mean difference in PET $H_2{}^{15}O$ MBF was 0.03 ± 0.14 mL/min/g and 0.02 ± 0.19 mL/min/g for infarcted and remote regions, respectively, and in PET $^{13}NH_3$ MBF was 0.03 ± 0.11 mL/min/g and 0.00 ± 0.09 mL/min/g for infarcted and remote regions, respectively. **Conclusion:** PET $H_2{}^{15}O$ and PET $^{13}NH_3$ resting MBF showed excellent reproducibility in a closed-chest animal model of chronic CAD. Resting PET $^{13}NH_3$ MBF was more reproducible than resting PET $H_2{}^{15}O$ MBF. A high level of reproducibility was maintained in areas of lower flow with infarction for both isotopes.

Key Words: blood flow; coronary disease; imaging; radioisotopes; PET

J Nucl Med 2006; 47:1193–1201

Several therapeutic advances have been developed for the treatment of chronic coronary artery disease (CAD) in patients otherwise not candidates for conventional revascularization. A common goal of these techniques, including laser revascularization, angiogenesis, and enhanced external counterpulsation, is to improve myocardial perfusion (*1–3*). However, demonstration of improved myocardial perfusion after these therapies has been challenging, in part due to limited knowledge on the reproducibility of serial blood flow measurements.

PET has distinct advantages for evaluating serial changes in myocardial blood flow (MBF). The noninvasive nature, along with the high spatial and temporal resolution, scatter and attenuation correction, high-energy tracers, and radiolabeling of naturally occurring compounds permit tracer kinetic modeling and accurate quantification of absolute MBF in mL/min/g. The short physical half-lives of PET tracers also allow repeated measurements of MBF in a single session. The PET perfusion tracers $H_2{}^{15}O$ and $^{13}NH_3$ are increasingly used in clinical and research settings for assessment of absolute MBF. Although absolute MBF with both isotopes has been validated under normal, ischemic, and nonreperfused infarction conditions (*4–11*), their short-term reproducibility is not well established for conditions of chronic CAD. In particular, reproducibility of PET MBF has been reported only for models with 3 or 4 myocardial segments, not for the standard 16-segment model. Detailed knowledge of the variability associated with these measurements is required for sensitivity and sample-size calculations.

Received Jan. 6, 2006; revision accepted Mar. 20, 2006.
For correspondence or reprints contact: Panithaya Chareonthaitawee, MD, Mayo Clinic, 200 First St. SW, Rochester, MN 55905.
E-mail: chareonthaitawee.panithaya@mayo.edu

Therefore, the aim of the study was to compare the short-term reproducibility of PET $H_2{}^{15}O$ MBF and PET $^{13}NH_3$ MBF in 16 standard myocardial segments in a closed-chest swine model of chronic CAD.

MATERIALS AND METHODS

Animal Experimental Preparation

The Institutional Animal Care and Use Committee approved these studies. The investigation conforms with the *Guide for the Care and Use of Laboratory Animals* (*12*). Figure 1 illustrates the protocol sequence. On day 1, each *Sus scrofa* swine (mean weight ± SD, 38 ± 5 kg) underwent general anesthesia, mechanical ventilation, and arterial hemodynamic monitoring. Each animal received an intravenous bolus (10,000 units) of unfractionated heparin before undergoing selective baseline coronary angiography via the left carotid artery. Under fluoroscopic guidance and sterile conditions, a copper stent was placed percutaneously in the mid left circumflex coronary artery. The copper stent produces an intense inflammatory fibrotic reaction and vessel remodeling linearly related to the period of exposure (*13,14*). The result is progressive coronary artery luminal narrowing, subtotal and total coronary occlusion, with collateral development to an area of nonviable myocardium, confirmed postmortem by staining with triphenyltetrazolium chloride (TTC). After stent placement, the wound was closed and the animal was allowed to recover. Analgesics and penicillin (900,000 units intramuscularly) were administered through day 3 and oral aspirin (325 mg/d) and oral amiodarone (5 mg/kg/d) through day 28 after the procedure.

On day 28, each animal again underwent general anesthesia, mechanical ventilation, and arterial hemodynamic monitoring before returning to the fluoroscopy suite. Selective coronary angiography was performed to confirm the reactive inflammatory fibrotic effect of the copper stent before PET scanning.

PET Scanning Protocol

Scans were performed with an Advance PET scanner (GE Healthcare). Animals were positioned in the scanner, and after exposure from ^{68}Ge rod sources, a 2-min transmission scan was acquired to determine the optimal positioning of the left ventricle (LV). A low-power laser beam was then superimposed on a cross-shaped ink mark on the animal to maintain the position. A 6-min transmission scan was performed for attenuation correction of the emission images. Emission images were acquired in the sequence shown in Figure 1. For the first resting $H_2{}^{15}O$ ($H_2{}^{15}O$ 1), an $H_2{}^{15}O$ bolus (711 ± 129 MBq) was injected intravenously over 20 s at a rate of 10 mL/min. The venous line was flushed for another 2 min. The following acquisition was used: 5 × 2, 20 × 3, 6 × 10, 6 × 30 frames × seconds. Hemodynamic measurements were obtained at the peak $H_2{}^{15}O$ activity. The second resting $H_2{}^{15}O$ bolus (691 ± 126 MBq) was administered 14 ± 2 min after the first $H_2{}^{15}O$ bolus and the image acquisition was repeated. After a period of 55 ± 4 min for $^{13}NH_3$ production, the first $^{13}NH_3$ slow bolus (709 ± 28 MBq) was injected intravenously over 20 s followed by a saline flush. The following acquisition parameters were used: 5 × 2, 20 × 3, 9 × 10, 4 × 20, 3 × 300 frames × seconds. Hemodynamic measurements were obtained at peak $^{13}NH_3$. After radioactive decay and additional $^{13}NH_3$ production (56 ± 5 min), the second $^{13}NH_3$ slow bolus (670 ± 46 MBq) was administered and the above $^{13}NH_3$ acquisition repeated.

After the PET scans, the animal was sacrificed and ex vivo procedures were performed. The heart was removed and divided into 5 or 6 short-axis slices of equal thickness. Heart slices were subsequently stained with 1% TTC and digitally photographed (Fig. 2).

PET Data Analysis

Sinograms were corrected for attenuation, scatter, randoms, dead time, and radioactive decay and reconstructed using filtered backprojection with a ramp filter (cutoff, 4 mm) into a 22-cm field of view. Images were transferred to a personal computer workstation and analyzed with commercial software (version 2.4; PMOD Technologies). Using a combination of long- and short-axis images, the operator defined the apex and the base of the LV myocardium: apex = the short-axis slice after visualization of the LV cavity and base = the slice at 2-slice thicknesses before visualization of the septal dropout (Fig. 3A). Each short-axis slice thickness was 4.25 mm. On short-axis $H_2{}^{15}O$ and $^{13}NH_3$ images, the center of the LV cavity and the septum were manually defined (Fig. 3A). The software then automatically defined 4 myocardial regions of interest (ROIs) in the apical planes and 6 myocardial ROIs in both mid and basal LV planes to produce a total of 16 myocardial segments (Fig. 3B). The left and right ventricular blood-pool ROIs were also defined manually on 3 short-axis planes to obtain the arterial and venous input functions, respectively (Fig. 3C). Factor analysis was applied to the $H_2{}^{15}O$ data to generate myocardial and blood-pool images (Fig. 4A) to guide

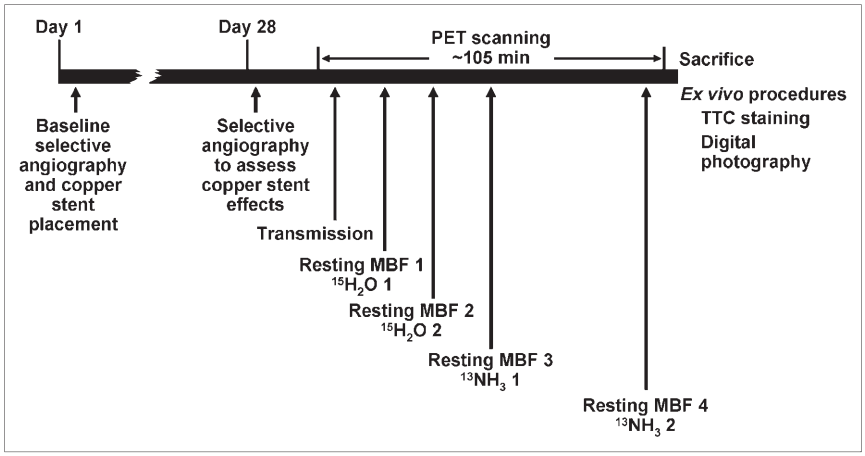

FIGURE 1. Protocol sequence. MBF = myocardial blood flow; TTC = triphenyltetrazolium chloride.

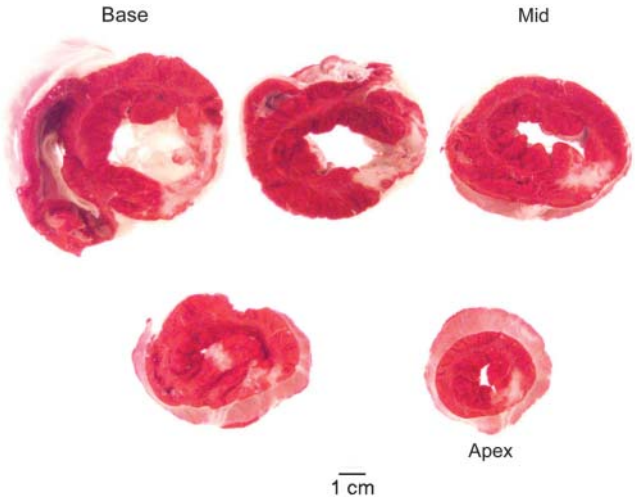

FIGURE 2. Pig pathologic specimen after processing with TTC.

$H_2{}^{15}O$ ROI placement (*15*). Time–activity curves were generated for the arterial, venous, and myocardial ROIs (Fig. 4B). The $H_2{}^{15}O$ arterial, venous and tissue input functions were fit to a 1-compartment model that includes left and right ventricle spillover corrections to yield values of regional and global MBF in mL/min/mL (*16*). Calculation of the tissue fraction (TF) was performed as previously described (*17*). The $^{13}NH_3$ input functions were fit to a 1-compartment model that includes metabolite and left and right ventricle spillover corrections to yield values of regional and global MBF in mL/min/mL (*18*). Only the first 4 min of the $^{13}NH_3$ time–activity curves were used in the modeling. For comparison with previously reported values, MBF values were divided by the density of myocardial tissue (1.04 g/mL) to express MBF values in mL/min/g (*19*).

To account for changes produced by cardiac workload, MBF was corrected for the rate·pressure product (RPP) (*20*), using the formula $MBF_{corr} = (MBF/RPP) \times 10^4$.

Statistical Analysis

Values are expressed as mean ± SD. Comparisons of the hemodynamic and MBF measurements were performed by paired Student *t* test. To determine the reproducibility of PET MBF, the repeatability coefficient (1.96 × SD) and limits of agreement were calculated as proposed by Bland and Altman (*21*). Absolute and percent mean differences were also calculated. ANOVA and post hoc analyses were used to determine the differences between MBF and TF values in infarcted versus remote regions.

RESULTS

Sixteen animals were included. Four animals died suddenly after copper stent placement, leaving 12 animals to undergo PET. The mean luminal coronary artery stenosis for the 12 animals was 91% ± 7%. All animals had evidence of myocardial infarction by TTC staining, exemplified by the processed short-axis slices of an animal from the study (Fig. 2).

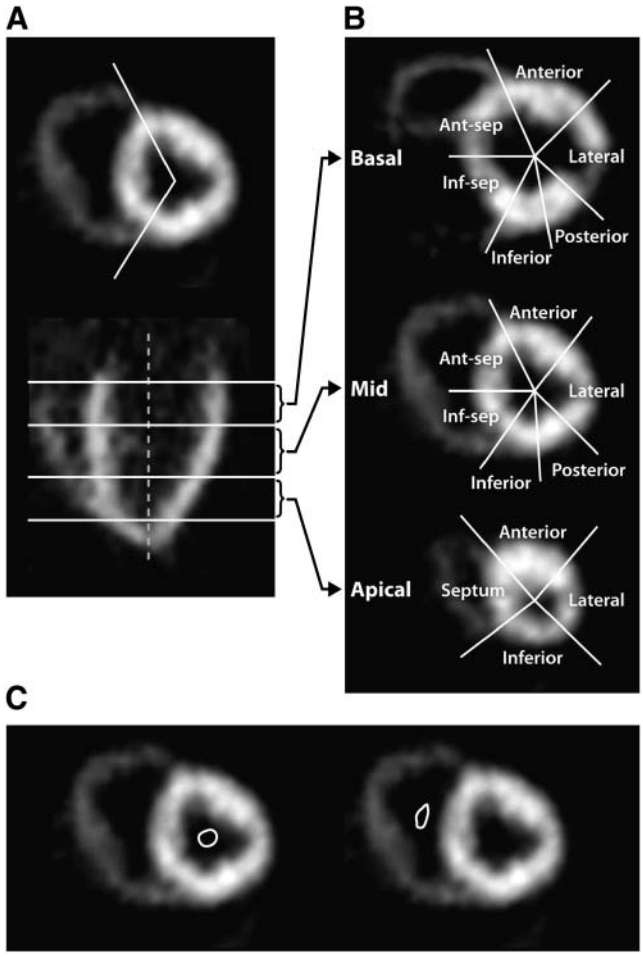

FIGURE 3. (A) Using a combination of long-axis and short-axis images, the operator defined the apex and the base of LV myocardium: the short-axis slice after visualization of LV cavity was chosen as apex and the slice at 2-slice thicknesses before visualization of the septal dropout was chosen as base. On a short-axis image, center of LV cavity and septum were manually defined. (B) Software subsequently automatically defined 4 myocardial ROIs in the apical planes, and 6 ROIs in both mid and basal LV planes to produce a total of 16 myocardial segments. Ant-sep = anteroseptal; Inf-sep = inferoseptal. (C) Left and right ventricular blood-pool ROIs were also defined manually on at least 3 short-axis planes to obtain the arterial and venous input functions, respectively

Hemodynamic Measurements

During the first and second MBF measurements for each PET perfusion tracer, the heart rate and the systolic and diastolic blood pressures were nearly identical (Table 1). There were no significant differences in the hemodynamic parameters between $H_2{}^{15}O$ 1 versus $H_2{}^{15}O$ 2 or between $^{13}NH_3$ 1 versus $^{13}NH_3$ 2. The RPP mean difference was 438 mm Hg × bpm (5.3% ± 9.6%) for $H_2{}^{15}O$ and 382 mm Hg × bpm (5.4% ± 15.5%) for $^{13}NH_3$.

Global MBF

Resting global MBF (i.e., mean flow in the whole LV) was 0.75 ± 0.26 mL/min/g for $H_2{}^{15}O$ 1, 0.76 ± 0.28

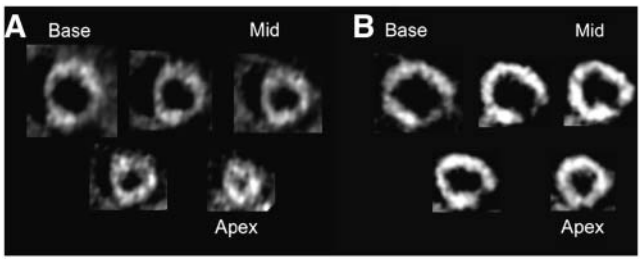

FIGURE 4. $H_2{}^{15}O$ (A) and $^{13}NH_3$ (B) short-axis images corresponding to pig pathologic specimen in Figure 2. Factor analysis was applied to $H_2{}^{15}O$ data to generate images for $H_2{}^{15}O$ ROI placement.

mL/min/g for $H_2{}^{15}O$ 2, 0.66 ± 0.19 mL/min/g for $^{13}NH_3$ 1, and 0.64 ± 0.22 mL/min/g for $^{13}NH_3$ 2. The mean difference was 0.01 ± 0.11 mL/min/g (1.4% ± 14.1%) for $H_2{}^{15}O$ MBF and 0.02 ± 0.09 mL/min/g (3.0% ± 13.0%) for $^{13}NH_3$ MBF. The repeatability coefficient was 0.21 mL/min/g (26.6% of the mean) and 0.18 mL/min/g (26.6% of the mean) for uncorrected global $H_2{}^{15}O$ and $^{13}NH_3$ MBF, respectively.

Corrected global MBF was higher than uncorrected MBF, with mean values of 1.14 ± 0.18 mL/min/g for $H_2{}^{15}O$ 1, 1.24 ± 0.24 mL/min/g for $H_2{}^{15}O$ 2, 1.03 ± 0.38 mL/min/g for $^{13}NH_3$ 1, and 1.18 ± 0.48 mL/min/g for $^{13}NH_3$ 2. The mean difference was 0.10 ± 0.18 mL/min/g (9.6% ± 15.7%) for corrected $H_2{}^{15}O$ global MBF and 0.15 ± 0.37 mL/min/g (18.6% ± 45.6%) for corrected $^{13}NH_3$ global MBF. The repeatability coefficient was 0.38 mL/min/g (30.7% of the mean) and 0.78 mL/min/g (67.8% of the mean) for corrected global $H_2{}^{15}O$ and $^{13}NH_3$ MBF, respectively.

Regional MBF

Resting uncorrected PET MBF values in 16 segments are shown in Table 2 with their mean differences and repeatability coefficients. Bland–Altman plots for resting regional uncorrected PET $H_2{}^{15}O$ MBF and PET $^{13}NH_3$ MBF are shown in Figure 5. The mean difference was 0.01 ± 0.18 mL/min/g and 0.01 ± 0.11 mL/min/g, with confidence limits of ± 0.36 and ± 0.22 mL/min/g for uncorrected regional PET $H_2{}^{15}O$ MBF and for uncorrected regional PET $^{13}NH_3$ MBF, respectively. The repeatability coefficient ranged from 0.20 to 0.60 mL/min/g (28.7%–72.1% of the mean) for uncorrected regional PET $H_2{}^{15}O$ MBF and from 0.17 to 0.32 mL/min/g (27.2%–51.1% of the mean) for uncorrected regional PET $^{13}NH_3$ MBF. The agreement in regional uncorrected MBF by each isotope is also shown in the scatter plots (Fig. 6).

Because animals underwent copper stent placement with its attendant progressive coronary artery narrowing in the proximal to mid left circumflex coronary artery, the posterior region of the LV contained infarcted tissue by TTC staining (Fig. 2). Resting uncorrected MBF measurements in these segments were significantly lower than those in remote regions. For $H_2{}^{15}O$ 1, mean infarcted MBF was 0.69 ± 0.28 mL/min/g versus mean remote MBF of 0.81 ± 0.30 mL/min/g ($P = 0.039$). For $H_2{}^{15}O$ 2, mean infarcted MBF was 0.68 ± 0.30 mL/min/g versus mean remote MBF of 0.82 ± 0.30 mL/min/g ($P = 0.019$). For $^{13}NH_3$ 1, mean infarcted MBF was 0.58 ± 0.20 mL/min/g versus mean remote MBF of 0.72 ± 0.22 mL/min/g ($P = 0.001$). For $^{13}NH_3$ 2, mean infarcted MBF was 0.58 ± 0.23 mL/min/g versus mean remote MBF of 0.71 ± 0.24 mL/min/g ($P = 0.005$). The mean difference in PET $H_2{}^{15}O$ MBF was 0.03 ± 0.14 mL/min/g and 0.02 ± 0.19 mL/min/g for infarcted and remote regions, respectively, and in PET $^{13}NH_3$ MBF was 0.03 ± 0.11 mL/min/g and 0.00 ± 0.09 mL/min/g for infarcted and remote regions, respectively.

The repeatability coefficients were similar between infarcted versus remote $H_2{}^{15}O$ MBF and similar between infarcted versus remote $^{13}NH_3$ MBF.

After RPP correction, the mean difference in regional corrected MBF ranged from 0.02 ± 0.27 mL/min/g (0.4% ± 30.2%) to 0.26 ± 0.60 mL/min/g (22.8% ± 47.8%) for $H_2{}^{15}O$ and from 0.08 ± 0.38 mL/min/g (14.9% ± 48.9%) to 0.22 ± 0.43 (26.1% ± 49.2%) for $^{13}NH_3$ corrected MBF (Table 3). Repeatability coefficients ranged from 0.38 to 1.19 mL/min/g (29.3%–76.1% of the mean) for $H_2{}^{15}O$ and from 0.70 to 0.98 mL/min/g (62.3%–83.4% of the mean) for $^{13}NH_3$. RPP correction appeared to worsen the reproducibility of regional MBF to a greater extent for $^{13}NH_3$ than for $H_2{}^{15}O$, shown by the Bland–Altman and scatter plots (Figs. 7 and 8).

TABLE 1
Hemodynamic Measurements

Measurement	$H_2{}^{15}O$ 1	$H_2{}^{15}O$ 2	*P*	$^{13}NH_3$ 1	$^{13}NH_3$ 2	*P*
HR	58 ± 20	57 ± 21	NS	61 ± 25	59 ± 25	NS
SBP	117 ± 12	113 ± 12	NS	107 ± 11	106 ± 14	NS
DBP	78 ± 14	75 ± 11	NS	70 ± 16	67 ± 18	NS
RPP	6,732 ± 2,490	6,294 ± 2,162	NS	6,454 ± 2,593	6,071 ± 2,440	NS

HR = heart rate (bpm); SBP = systolic blood pressure (mm Hg); DBP = diastolic blood pressure (mm Hg); RPP = rate·pressure product (HR × SBP).

Data are expressed as mean ± SD.

TABLE 2
Resting Regional Uncorrected MBF (mL/min/g)

Segment	$H_2{}^{15}O$ 1	$H_2{}^{15}O$ 2	Mean difference		Repeatability coefficient		$^{13}NH_3$ 1	$^{13}NH_3$ 2	Mean difference		Repeatability coefficient	
			Absolute	%	Absolute	% of mean			Absolute	%	Absolute	% of mean
Apical anterior	0.71 ± 0.30	0.77 ± 0.27	−0.06 ± 0.15	12.5 ± 26.7	0.30	39.0	0.61 ± 0.17	0.64 ± 0.23	−0.03 ± 0.11	2.7 ± 17.3	0.21	32.3
Apical lateral	0.76 ± 0.28	0.77 ± 0.33	−0.01 ± 0.17	0.2 ± 21.0	0.33	41.4	0.56 ± 0.16	0.55 ± 0.21	0.02 ± 0.11	4.1 ± 18.7	0.22	38.2
Apical inferior	0.84 ± 0.26	0.83 ± 0.28	0.01 ± 0.19	0.5 ± 21.0	0.38	43.8	0.61 ± 0.19	0.60 ± 0.26	0.01 ± 0.16	2.4 ± 23.8	0.32	51.1
Apical septal	0.85 ± 0.33	0.86 ± 0.28	−0.01 ± 0.30	8.3 ± 33.5	0.58	65.0	0.70 ± 0.20	0.69 ± 0.24	0.01 ± 0.11	2.5 ± 13.8	0.21	29.1
Mid anterior	0.75 ± 0.26	0.77 ± 0.32	−0.02 ± 0.19	3.3 ± 23.7	0.39	49.3	0.64 ± 0.20	0.63 ± 0.22	0.00 ± 0.09	0.3 ± 12.6	0.18	27.2
Mid lateral	0.71 ± 0.27	0.74 ± 0.29	0.03 ± 0.14	4.6 ± 22.1	0.27	36.0	0.60 ± 0.20	0.57 ± 0.22	0.03 ± 0.11	4.7 ± 21.2	0.22	36.2
Mid posterior	0.64 ± 0.28	0.65 ± 0.24	−0.01 ± 0.12	6.0 ± 26.0	0.24	35.9	0.55 ± 0.20	0.56 ± 0.25	0.00 ± 0.11	0.9 ± 19.6	0.22	38.2
Mid inferior	0.67 ± 0.23	0.67 ± 0.26	0.00 ± 0.10	2.2 ± 16.3	0.20	28.7	0.66 ± 0.21	0.63 ± 0.25	0.02 ± 0.13	3.4 ± 18.7	0.25	37.3
Mid inferoseptal	0.78 ± 0.32	0.82 ± 0.27	−0.04 ± 0.30	14.7 ± 47.3	0.60	72.1	0.68 ± 0.20	0.69 ± 0.26	−0.01 ± 0.14	0.4 ± 16.9	0.28	39.2
Mid anteroseptal	0.78 ± 0.24	0.81 ± 0.30	−0.03 ± 0.15	3.3 ± 21.0	0.30	36.5	0.75 ± 0.21	0.72 ± 0.25	0.03 ± 0.12	3.7 ± 16.3	0.25	32.7
Basal anterior	0.75 ± 0.27	0.78 ± 0.32	−0.03 ± 0.16	2.9 ± 22.5	0.32	40.2	0.67 ± 0.23	0.65 ± 0.23	0.02 ± 0.10	2.1 ± 15.0	0.20	29.1
Basal lateral	0.67 ± 0.24	0.66 ± 0.27	0.01 ± 0.20	0.5 ± 27.9	0.40	57.7	0.60 ± 0.18	0.55 ± 0.20	0.04 ± 0.13	6.0 ± 20.4	0.27	45.2
Basal posterior	0.59 ± 0.27	0.54 ± 0.27	0.05 ± 0.12	8.2 ± 24.0	0.24	40.9	0.56 ± 0.22	0.56 ± 0.24	0.00 ± 0.09	0.3 ± 14.4	0.17	29.3
Basal inferior	0.67 ± 0.25	0.76 ± 0.33	−0.09 ± 0.22	17.3 ± 43.2	0.44	59.6	0.69 ± 0.25	0.68 ± 0.23	0.02 ± 0.13	0.7 ± 21.5	0.27	28.1
Basal inferoseptal	0.78 ± 0.31	0.72 ± 0.27	0.06 ± 0.22	3.5 ± 28.8	0.44	56.3	0.72 ± 0.25	0.69 ± 0.25	0.03 ± 0.11	1.8 ± 15.3	0.22	29.9
Basal anteroseptal	0.83 ± 0.34	0.81 ± 0.35	0.02 ± 0.15	1.7 ± 15.5	0.29	34.0	0.77 ± 0.23	0.73 ± 0.25	0.04 ± 0.11	4.3 ± 14.3	0.22	28.2

Data are expressed as mean ± SD.

TF

TF in regions subtended by the stented artery was significantly lower than that in remote regions (0.536 ± 0.134 g/mL vs. 0.782 ± 0.073 g/mL, $P < 0.0001$) for $H_2{}^{15}O$ 1. The range of $H_2{}^{15}O$ 1 TF was 0.287–0.773 g/mL in segments containing TTC-negative tissue and 0.556–0.950 g/mL in remote myocardium. For $H_2{}^{15}O$ 2, TF was 0.574 ± 0.127 (range, 0.325–0.679) g/mL in stented vs. 0.792 ± 0.081 (range, 0.593–0.894) g/mL in remote regions.

DISCUSSION

Our results indicate that MBF measurements in absolute terms obtained noninvasively with PET $H_2{}^{15}O$ and PET $^{13}NH_3$ in a single session were highly reproducible in a swine model of chronic CAD. The high level of reproducibility was found in both normal- and low-flow states, the latter containing infarcted myocardium, and was present for global and regional MBF measurements by both isotopes. However, $^{13}NH_3$ MBF was more reproducible than $H_2{}^{15}O$ MBF.

Reproducibility of PET $H_2{}^{15}O$ MBF

The reproducibility of PET $H_2{}^{15}O$ resting MBF has been reported in 3 publications to date. Two studies were from the same institution, and all 3 studies had small numbers of human subjects (11 and 21 healthy volunteers, and 15 patients with CAD) (*10,22,23*). The studies found very good reproducibility of resting PET $H_2{}^{15}O$ MBF but all 3 in effect reported values in a 4-segment model of the LV (septal, anterior, lateral, inferior). To our knowledge, the reproducibility of the clinically used 16-segment model has not been reported previously. Using the 16-segment model, we observed very good reproducibility of regional resting uncorrected PET $H_2{}^{15}O$ MBF, with a mean difference of 0.01 mL/min/g and absolute repeatability coefficients in the range of 0.24–0.60 mL/min/g or 28.7%–72.1% of the mean. Despite the 16-segment model, our values are similar to the previously reported reproducibility coefficients of 0.20–0.66 mL/min/g for resting PET $H_2{}^{15}O$ MBF using the 4-segment model (*10,22*).

Reproducibility of regional uncorrected resting PET $H_2{}^{15}O$ MBF in infarcted myocardium has not previously been reported. In our study, resting uncorrected PET $H_2{}^{15}O$ MBF in regions subtended by the copper-stented coronary artery and containing TTC-negative myocardium (repeatability coefficient, 0.24 mL/min/g) showed reproducibility similar to that of remote areas (repeatability coefficient, 0.39 mL/min/g). Flow values in these regions were higher than expected, likely from a contribution of residual antegrade and collateral flows and the admixture of scar tissue and viable myocardium. This was confirmed by a mean TF of 0.536 ± 0.134 g/mL in the same regions. Reproducibility of regional resting PET $H_2{}^{15}O$ MBF in ischemic territories has previously been reported to be 0.26 mL/min/g, or 24% of the mean; however, in that study, repeat measurements were obtained at 24 wk and a 4-segment model was used (*23*).

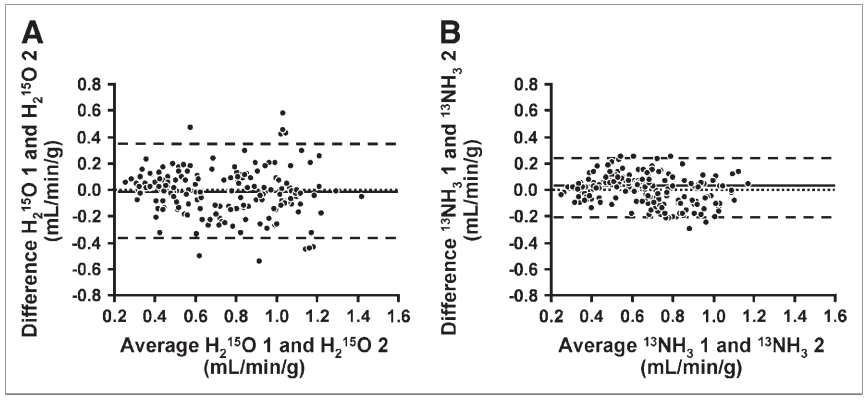

FIGURE 5. Bland–Altman plots for resting regional uncorrected MBF for $H_2^{15}O$ (A) and $^{13}NH_3$ (B). Mean difference was 0.01 mL/min/g and 0.01 mL/min/g, with confidence limits of ±0.37 and ±0.23 mL/min/g for $H_2^{15}O$ and for $^{13}NH_3$, respectively.

Global resting PET $H_2^{15}O$ MBF showed excellent reproducibility in our study, with an absolute repeatability coefficient of 0.21 mL/min/g (27% of the mean), comparable to prior reports of 0.17 mL/min/g (18% of the mean) (*10*), 0.26 mL/min/g (21% of the mean) (*22*), and 0.25 mL/min/g (23% of the mean) (*23*).

A wide range of uncorrected resting global and regional PET $H_2^{15}O$ MBF in remote myocardium has been reported in healthy humans and animals (*10,24–27*). The mean global and regional resting PET $H_2^{15}O$ MBF values in the current study are in agreement with prior studies. RPP correction has not consistently reduced the variability associated with these measurements in our study or others (*10,25,28*), suggesting the contribution of other factors. Heterogeneity of resting MBF has been described within and between individuals (*25*). Both temporal and spatial heterogeneity have been observed in healthy humans and animals and may relate to "twinkling" of capillary flows, time-dependent changes in regional metabolic requirements, local autoregulatory changes, and the fractal nature of regional flow distribution (*25,29*).

Reproducibility of PET $^{13}NH_3$ MBF

Three prior publications have addressed the reproducibility of resting PET $^{13}NH_3$ MBF measurements (*11,18,28*). These studies included 6, 8, and 30 healthy volunteers, and 6 humans with stable CAD (*28*). Important differences between these reports and the current study include their use of human subjects, their longer time interval between scans, their fewer myocardial regions (3–4), and the 3-compartment kinetic modeling in 2 earlier studies. Despite smaller ROIs, our mean difference (0.00–0.04 mL/min/g) between the 2 resting regional PET $^{13}NH_3$ MBF was similar to the mean difference in the earlier study (0.04 ± 0.04 mL/min/g) (*28*). Use of anesthetized animals likely contributed in part to our observed reproducibility by minimizing subject motion, allowing more stringent hemodynamic regulation and reducing other effects of consciousness on blood flow and autoregulatory mechanisms. RPP correction did not improve the reproducibility of resting regional PET $^{13}NH_3$ MBF in their study or our study. The mean difference of 15.8% ± 15.8% between the 2 resting PET $^{13}NH_3$ MBF values in the second study (*11*) is higher than the mean difference in our study (0.3%–6.0%), despite our smaller ROIs. That study was among the few in which RPP correction improved reproducibility of resting PET $^{13}NH_3$ MBF. In the study examining 1- and 2-compartmental modeling techniques in healthy humans, the relative change between the 2 resting MBF indices for all techniques was 0.03–0.04 mL/min/g but that study reported MBF values in only 3 myocardial segments (*18*).

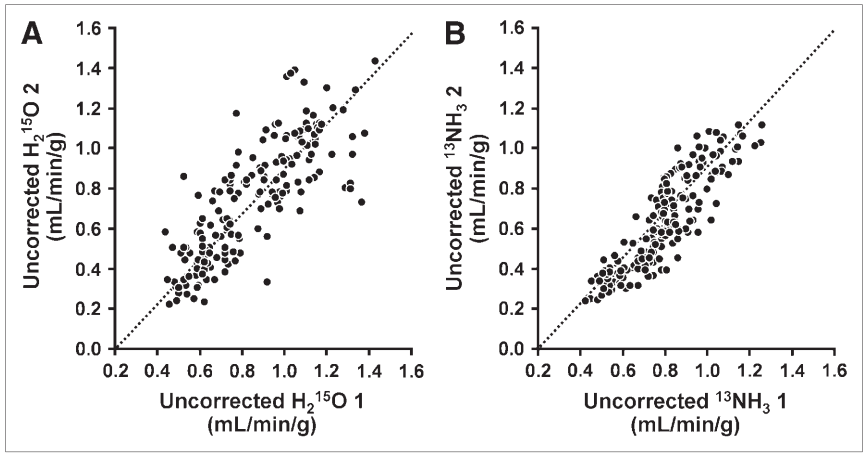

FIGURE 6. Scatter plots for $H_2^{15}O$ (A) and $^{13}NH_3$ (B) uncorrected PET MBF. Line of identity is shown.

TABLE 3
Resting Regional RPP-Corrected MBF (mL/min/g)

Segment	$H_2{}^{15}O$ 1	$H_2{}^{15}O$ 2	Mean difference		Repeatability coefficient		$^{13}NH_3$ 1	$^{13}NH_3$ 2	Mean difference		Repeatability coefficient	
			Absolute	%	Absolute	% of mean			Absolute	%	Absolute	% of mean
Apical anterior	1.06 ± 0.22	1.25 ± 0.26	−0.20 ± 0.27	21.7 ± 28.6	0.54	44.9	0.96 ± 0.34	1.18 ± 0.51	−0.22 ± 0.43	26.1 ± 49.2	0.86	77.4
Apical lateral	1.15 ± 0.21	1.23 ± 0.28	−0.08 ± 0.20	7.6 ± 17.4	0.40	32.4	0.88 ± 0.35	0.99 ± 0.41	−0.11 ± 0.35	17.6 ± 47.3	0.70	71.9
Apical inferior	1.30 ± 0.34	1.35 ± 0.29	−0.05 ± 0.25	7.0 ± 21.3	0.51	37.0	0.95 ± 0.36	1.06 ± 0.43	−0.12 ± 0.43	19.7 ± 54.4	0.85	81.2
Apical septal	1.31 ± 0.48	1.43 ± 0.32	−0.12 ± 0.51	16.3 ± 32.3	1.02	71.5	1.09 ± 0.41	1.28 ± 0.55	−0.20 ± 043	21.3 ± 47.0	0.85	68.8
Mid anterior	1.13 ± 0.21	1.23 ± 0.24	−0.11 ± 0.26	11.2 ± 24.1	0.53	43.3	0.98 ± 0.34	1.15 ± 0.46	−0.17 ± 0.36	21.1 ± 43.7	0.73	65.9
Mid lateral	1.06 ± 0.24	1.17 ± 0.26	−0.12 ± 0.25	13.4 ± 26.1	0.50	43.1	0.96 ± 0.39	1.03 ± 0.42	−0.08 ± 0.38	14.9 ± 48.9	0.76	73.4
Mid posterior	0.94 ± 0.21	1.06 ± 0.30	−0.12 ± 0.27	14.8 ± 30.3	0.54	51.7	0.85 ± 0.36	1.00 ± 0.47	−0.15 ± 0.39	22.4 ± 50.9	0.78	80.9
Mid inferior	1.02 ± 0.20	1.09 ± 0.33	−0.07 ± 0.22	6.1 ± 20.2	0.44	40.1	1.02 ± 0.37	1.18 ± 0.50	−0.16 ± 0.42	18.8 ± 47.0	0.83	72.6
Mid inferoseptal	1.17 ± 0.28	1.42 ± 0.60	−0.26 ± 0.60	22.8 ± 47.8	1.19	88.3	1.07 ± 0.39	1.27 ± 0.54	−0.21 ± 0.41	22.8 ± 45.3	0.83	68.3
Mid anteroseptal	1.18 ± 0.21	1.31 ± 0.32	−0.14 ± 0.34	13.1 ± 29.6	0.71	54.7	1.19 ± 0.47	1.33 ± 0.54	−0.14 ± 0.47	17.6 ± 45.7	0.94	71.7
Basal anterior	1.14 ± 0.24	1.24 ± 0.29	−0.11 ± 0.27	11.1 ± 25.1	0.54	43.6	1.04 ± 0.38	1.20 ± 0.53	−0.16 ± 0.45	19.8 ± 50.2	0.90	74.0
Basal lateral	1.03 ± 0.29	1.09 ± 0.37	−0.06 ± 0.42	9.6 ± 33.7	0.84	76.1	0.96 ± 0.39	1.03 ± 0.45	−0.08 ± 0.43	15.9 ± 55.7	0.86	83.4
Basal posterior	0.91 ± 0.30	0.89 ± 0.34	0.02 ± 0.27	0.4 ± 30.2	0.55	59.1	0.90 ± 0.46	1.05 ± 0.53	−0.16 ± 0.37	21.5 ± 51.5	0.74	73.0
Basal inferior	1.01 ± 0.23	1.24 ± 0.41	−0.24 ± 0.41	25.9 ± 42.9	0.81	65.4	1.08 ± 0.41	1.26 ± 0.55	−0.19 ± 0.49	23.0 ± 57.3	0.98	80.6
Basal inferoseptal	1.17 ± 0.22	1.21 ± 0.41	−0.04 ± 0.37	4.7 ± 32.9	0.75	57.4	1.10 ± 0.41	1.28 ± 0.53	−0.19 ± 0.39	20.4 ± 39.8	0.77	62.3
Basal anteroseptal	1.23 ± 0.26	1.28 ± 0.25	−0.06 ± 0.19	6.0 ± 14.8	0.38	29.3	1.22 ± 0.46	1.35 ± 0.56	−0.14 ± 0.44	15.7 ± 41.6	0.88	65.8

Data are expressed as mean ± SD.

In the current study, the repeatability coefficient of resting PET $^{13}NH_3$ MBF in regions containing TTC-negative myocardium (0.22 mL/min/g) was similar to that of remote areas (0.18 mL/min/g), suggesting stable reproducibility in areas of low flow with infarction.

Resting PET $^{13}NH_3$ MBF in remote or normal regions is in agreement with prior measurements (*11,28*). Interestingly, PET $^{13}NH_3$ MBF estimates appear to be consistently lower than PET $H_2{}^{15}O$ MBF estimates in this study. In the single prior publication comparing PET $H_2{}^{15}O$ MBF and PET $^{13}NH_3$ MBF, this systematic difference was not present in the 15 healthy volunteers (*9*). The reasons for the difference in our study are likely both physiologic and methodologic. First, in all animals, PET image acquisition was first performed with the 2 serial $H_2{}^{15}O$ administrations, followed almost 1 h later by the first $^{13}NH_3$ acquisition. With prolonged instrumentation and sedation, a trend toward lower blood pressure was observed over the course of our PET, which might have contributed to lower resting MBF. Second, metabolite correction was applied to the $^{13}NH_3$ data and might systematically affect MBF estimates. However, only the first 4 min of data were used in the kinetic modeling, and at 4 min there remains ~75% of the ^{13}N-labeled radioactivity as $^{13}NH_3$ in the arterial blood of human volunteers (*30*). Third, if the tissue composition is highly heterogeneous, with a mixture of viable and fibrotic myocardium, PET $^{13}NH_3$ MBF may be lower than PET $H_2{}^{15}O$ MBF because the former reflects the average uptake and therefore average flow in the admixture, whereas $H_2{}^{15}O$ uptake is negligible in scar and mainly reflects activity in the better perfused segments (*31*). Though this might explain the lower PET $^{13}NH_3$ MBF estimates in regions with this admixture, it does not account for the difference in MBF in normal regions. Whereas equivalence in performance of $H_2{}^{15}O$ and $^{13}NH_3$ as perfusion tracers may be demonstrated, the 2 tracers are not congruent. Myocardial $H_2{}^{15}O$ uptake does not vary despite wide variations on flow rate because it is metabolically inert and freely diffusible across capillary and sarcolemmal membranes (*32*). On the other hand, myocardial $^{13}NH_3$ uptake depends on blood flow, myocardial metabolic trapping, and whole-body metabolism of $^{13}NH_3$. Despite accounting for these differences in kinetic modeling, these tracers may still provide measurements of different parameters, even in normal myocardium.

Reproducibility of PET $H_2{}^{15}O$ MBF Versus PET $^{13}NH_3$ MBF

Although reproducibility was excellent for both PET $H_2{}^{15}O$ and PET $^{13}NH_3$ uncorrected resting MBF in the current study, reproducibility was higher for PET $^{13}NH_3$ than for PET $H_2{}^{15}O$ regional MBF (Fig. 5; Table 2). The short physical half-life of $H_2{}^{15}O$ (2.1 min vs. 9.8 min for $^{13}NH_3$) results in a rapid decline in counting rates, creating considerable statistical noise and affecting tracer quantification (*33*). The smaller ROIs in the current study compound the

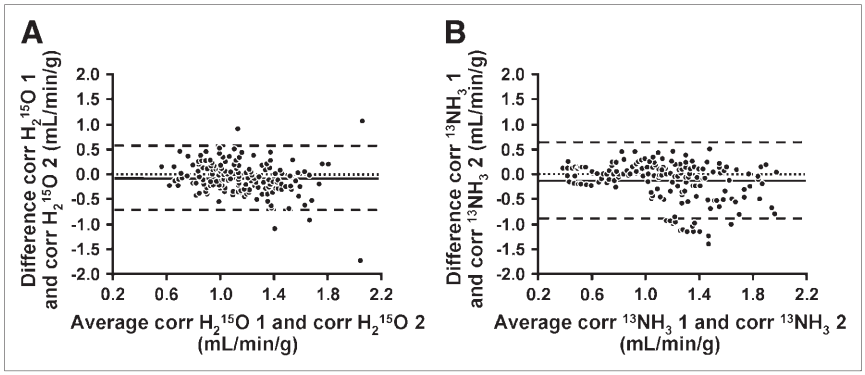

FIGURE 7. Bland–Altman plots for resting regional corrected MBF values for $H_2^{15}O$ (A) and $^{13}NH_3$ (B). Mean difference was 0.11 mL/min/g and 0.16 mL/min/g, with confidence limits of ±0.66 and ±0.80 mL/min/g for $H_2^{15}O$ and for $^{13}NH_3$, respectively. corr = corrected.

existing problem of statistical noise with $H_2^{15}O$. Subtraction for spillover between myocardium and blood pool also augments statistical noise and is sensitive to subject movement (*5*). The latter poses more challenges for ROI placement on $H_2^{15}O$ images than on $^{13}NH_3$ images because of the poorer myocardial definition of the former. Lastly, the partition coefficient of water may not be constant around infarcted tissue and may affect PET $H_2^{15}O$ MBF in such regions (*17*).

In areas of low flow with infarction (TTC-negative regions; Fig. 2), reproducibility remained excellent for both $H_2^{15}O$ and $^{13}NH_3$. Lower counting statistics associated with lower flow is a potential contributing factor to differences in reproducibility between remote and infarcted regions, particularly with the higher statistical noise of $H_2^{15}O$. With $^{13}NH_3$, differences in trapping and metabolism in areas of lower flow with infarction could alter the flow–extraction relationship. In particular, the cell-integrity dependence of $^{13}NH_3$ extraction may affect its reproducibility in TTC-negative regions. Lastly, partial-volume correction was not applied to our $H_2^{15}O$ or $^{13}NH_3$ studies; partial-volume effects can result in <100% recovery of tissue activity in structures measuring less than about twice the full width at half maximum spatial resolution and can amount to 30% activity loss (*34*). This may be a particular issue for regions containing infarcted myocardium.

Limitations

Because of practical considerations, the order of 2 tracers could not be randomized. Further, we did not assess reproducibility of hyperemic MBF in part due to practical considerations but also because the response of swine to vasodilator stress is highly variable in our experience. Even in humans, up to 16% of patients receiving adenosine at a dose of 140 μg/kg/min have failed to achieve maximal coronary vasodilation (*35*).

Because all animals underwent copper stent placement in only the mid left circumflex coronary artery, results may not be applicable to other regions of low flow with infarction or to the setting of multivessel disease.

CONCLUSION

PET $H_2^{15}O$ and PET $^{13}NH_3$ resting global and regional MBF showed excellent reproducibility in a closed-chest animal model of chronic CAD, despite small ROIs. Resting PET $^{13}NH_3$ MBF was more reproducible than resting PET $H_2^{15}O$ MBF, likely in large part due to higher counting statistics with $^{13}NH_3$. A high level of reproducibility was maintained in areas of low flow with infarction with both $^{13}NH_3$ and $H_2^{15}O$. RPP correction did not improve short-term reproducibility of either resting PET $^{13}NH_3$ MBF or resting PET $H_2^{15}O$ MBF, suggesting the role of other factors.

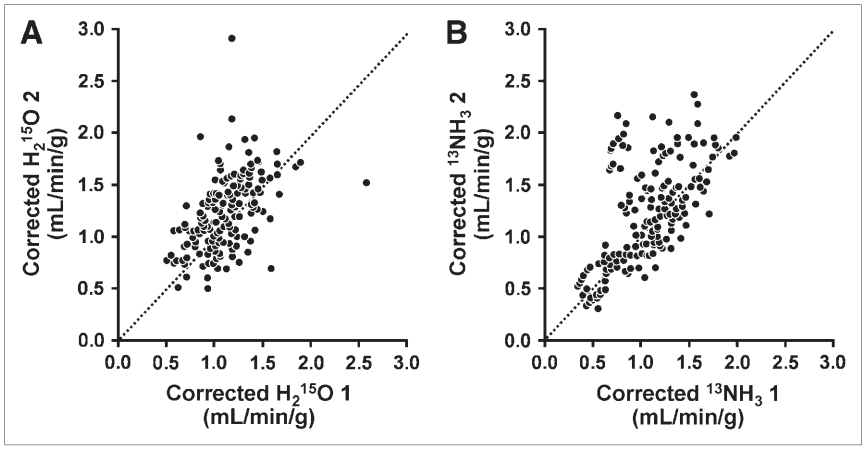

FIGURE 8. Regression plots for $H_2^{15}O$ (A) and $^{13}NH_3$ (B) corrected PET MBF. Line of identity is shown.

ACKNOWLEDGMENTS

The authors thank the Mayo Cyclotron personnel for isotope production, Mayo PET technologists for late-night acquisitions, and Teresa Decklever for her contribution to PET data analysis. We are also indebted to Drs. Alejandro R. Chade and Lilach O. Lerman for their support. The study was supported by a grant from the Mayo Foundation. This study was presented in part at the 9th Annual Symposium and Scientific Session of the American Society of Nuclear Cardiology, New York, NY, September 30 to October 2, 2004. The authors have no conflicts of interest to disclose.

REFERENCES

1. Freedman SB, Isner JM. Therapeutic angiogenesis for coronary artery disease. *Ann Intern Med.* 2002;136:54–71.
2. Frazier OH, March RJ, Horvath KA. Transmyocardial revascularization with a carbon dioxide laser in patients with end-stage coronary artery disease. *N Engl J Med.* 1999;341:1021–1028.
3. Arora RR, Chou TM, Jain D, et al. The multicenter study of enhanced external counterpulsation (MUST-EECP): effect of EECP on exercise-induced myocardial ischemia and anginal episodes. *J Am Coll Cardiol.* 1999;33:1833–1840.
4. Bol A, Melin JA, Vanoverschelde J-L, et al. Direct comparison of [^{13}N]ammonia and [^{15}O]water estimates of perfusion with quantification of regional myocardial blood flow by microspheres. *Circulation.* 1993;87:512–525.
5. Bergmann SR, Fox KA, Rand AL, et al. Quantification of regional myocardial blood flow in vivo with $H_2{}^{15}O$. *Circulation.* 1984;70:724–733.
6. Araujo LI, Lammertsma AA, Rhodes CG, et al. Noninvasive quantification of regional myocardial blood flow in coronary artery disease with oxygen-15-labeled carbon dioxide inhalation and positron emission tomography. *Circulation.* 1991;83:875–885.
7. Hutchins GD, Schwaiger M, Rosenspire KC, Krivokapich J, Schelbert H, Kuhl DE. Noninvasive quantification of regional blood flow in the human heart using N-13 ammonia and dynamic positron emission tomographic imaging. *J Am Coll Cardiol.* 1990;15:1032–1042.
8. Krivokapich J, Smith GT, Huang S, et al. N-13-ammonia myocardial imaging at rest and with exercise in normal volunteers: quantification of absolute myocardial perfusion with dynamic positron emission tomography. *Circulation.* 1989;80:1328–1337.
9. Nitzsche EU, Choi Y, Czernin J, Hoh CK, Huang SC, Schelbert HR. Noninvasive quantification of myocardial blood flow in humans: a direct comparison of the [^{13}N]ammonia and the [^{15}O]water techniques. *Circulation.* 1996;93:2000–2006.
10. Kaufmann PA, Gnecchi-Ruscone T, Yap JT, Rimoldi O, Camici PG. Assessment of the reproducibility of baseline and hyperemic myocardial blood flow measurements with oxygen-15 labeled water and PET. *J Nucl Med.* 1999;40:1848–1856.
11. Nagamachi S, Czernin J, Kim AS, et al. Reproducibility of measurements of regional resting and hyperemic myocardial blood flow assessed with PET. *J Nucl Med.* 1996;37:1626–1631.
12. National Research Council. *Guide for the Care and Use of Laboratory Animals*. NIH publication 85-23 (revised). Bethesda, MD: U.S. Department of Health and Human Services, National Institutes of Health; 1996.
13. Stabb ME, Meeker DK, Edwards WD, et al. Reliable models of severe coronary stenosis in porcine coronary arteries: lesion induction by high temperature or copper stent. *J Interv Cardiol.* 1997;10:61–69.
14. Chareonthaitawee P, O'Connor MK, Gibbons RJ, Ritman EL, Christian TF. The effect of collateral flow and myocardial viability on the distribution of technetium-99m sestamibi in a closed-chest model of coronary occlusion and reperfusion. *Eur J Nucl Med.* 2000;27:508–516.
15. Hermansen F, Ashburner J, Spinks TJ, Kooner JS, Camici PG, Lammertsma AA. Generation of myocardial factor images directly from the dynamic oxygen-15-water scan without use of an oxygen-15-carbon monoxide blood-pool scan. *J Nucl Med.* 1998;39:1696–1702.
16. Hermansen F, Rosen SD, Fath-Ordoubadi F, et al. Measurement of myocardial blood flow with oxygen-15 labelled water: comparison of different administration protocols. *Eur J Nucl Med.* 1998;25:751–759.
17. Iida H, Rhodes C, de Silva R, et al. Myocardial tissue fraction: correction for partial volume effects and measure of tissue viability. *J Nucl Med.* 1991;32:2169–2175.
18. DeGrado TR, Hanson MW, Turkington TG, et al. Estimation of myocardial blood flow for longitudinal studies with ^{13}N-labeled ammonia and positron emission tomography. *J Nucl Cardiol.* 1996;3:494–507.
19. Schèafers KP, Spinks TJ, Camici PG, et al. Absolute quantification of myocardial blood flow with $H_2{}^{15}O$ and 3-dimensional PET: an experimental validation. *J Nucl Med.* 2002;43:1031–1040.
20. Czernin J, Mèuller P, Chan S, et al. Influence of age and hemodynamics on myocardial blood flow and flow reserve. *Circulation.* 1993;88:62–69.
21. Bland JM, Altman DG. Statistical methods for assessing agreement between two methods of clinical measurement. *Lancet.* 1986;1:307–310.
22. Wyss CA, Koepfli P, Mikolajczyk K, Burger C, von Schulthess GK, Kaufmann PA. Bicycle exercise stress in PET for assessment of coronary flow reserve: repeatability and comparison with adenosine stress. *J Nucl Med.* 2003;44:146–154.
23. Jagathesan R, Kaufmann PA, Rosen SD, et al. Assessment of the long-term reproducibility of baseline and dobutamine-induced myocardial blood flow in patients with stable coronary artery disease. *J Nucl Med.* 2005;46:212–219.
24. Bergmann SR, Herrero P, Markham J, Weinhemer CJ, Walsh MN. Noninvasive quantitation of myocardial blood flow in human subjects with oxygen-15-labeled water and positron emission tomography. *J Am Coll Cardiol.* 1989;14:639–652.
25. Chareonthaitawee P, Kaufman PA, Rimoldi O, Camici PG. Heterogeneity of resting and hyperemic myocardial blood flow in healthy humans. *Cardiovasc Res.* 2001;50:151–161.
26. Iida H, Yokoyama I, Agostini D, et al. Quantitative assessment of regional myocardial blood flow using oxygen-15-labelled water and positron emission tomography: a multicentre evaluation in Japan. *Eur J Nucl Med.* 2000;27:192–201.
27. Katoh C, Morita K, Shiga T, Kubo N, Nakada K, Tamaki N. Improvement of algorithm for quantification of regional myocardial blood flow using ^{15}O-water with PET. *J Nucl Med.* 2004;45:1908–1916.
28. Sawada S, Muzik O, Beanlands RS, Wolfe E, Hutchins GD, Schwaiger M. Interobserver and interstudy variability of myocardial blood flow and flow-reserve measurements with nitrogen 13 ammonia-labeled positron emission tomography. *J Nucl Cardiol.* 1995;2:413–422.
29. Marcus ML, Kerber RE, Ehrhardt JE, Falsetti HL, Davis DM, Abboud FM. Spatial and temporal heterogeneity of left ventricular perfusion in awake dogs. *Am Heart J.* 1977;94:748–754.
30. Rosenspire KC, Schwaiger M, Mangner TJ, Hutchins GD, Sutorik A, Kuhl DE. Metabolic fate of N-13-ammonia in human and canine blood. *J Nucl Med.* 1990;31:163–167.
31. Rimoldi OE, Camici PG. Positron emission tomography for quantitation of myocardial perfusion. *J Nucl Cardiol.* 2004;11:482–490.
32. Kaufmann PA, Camici PG. Myocardial blood flow measurement by PET: technical aspects and clinical applications. *J Nucl Med.* 2005;46:75–88.
33. Schelbert HR, Czernin J, Huang SC. Quantitation of regional blood flow: oxygen-15-water versus nitrogen-13-ammonia. *J Nucl Med.* 1990;31:1431–1433.
34. Hoffman EJ, Huang SC, Phelps ME. Quantitation in positron emission computed tomography. 1. Effect of object size. *J Comput Assist Tomogr.* 1979;3:299–308.
35. Wilson RF, Wyche K, Christensen BV, Zimmer S, Laxson DD. Effects of adenosine on human coronary arterial circulation. *Circulation.* 1990;82:1595–1606.

The Journal of NUCLEAR MEDICINE

Reproducibility of Measurements of Regional Myocardial Blood Flow in a Model of Coronary Artery Disease: Comparison of $H_2{}^{15}O$ and $^{13}NH_3$ PET Techniques

Panithaya Chareonthaitawee, Stuart D. Christenson, Jill L. Anderson, Brad J. Kemp, David O. Hodge, Erik L. Ritman and Raymond J. Gibbons

J Nucl Med. 2006;47:1193-1201.

The Journal of Nuclear Medicine is published monthly.
SNMMI | Society of Nuclear Medicine and Molecular Imaging
1850 Samuel Morse Drive, Reston, VA 20190.
(Print ISSN: 0161-5505, Online ISSN: 2159-662X)

SNMMI SOCIETY OF NUCLEAR MEDICINE AND MOLECULAR IMAGING